Nanotechnology **19** (2008) 384009 (9pp) doi:10.1088/0957-4484/19/38/384009

Anisotropic diffusion of point defects in a two-dimensional crystal of streptavidin observed by high-speed atomic force microscopy

Daisuke Yamamoto, Takayuki Uchihashi, Noriyuki Kodera and Toshio Ando[1]

Department of Physics, Kanazawa University, Kakuma-machi, Kanazawa 920-1192, Japan
and
Core Research for Evolutional Science and Technology (CREST) of the Japan Science and Technology Agency (JST), Sanbon-cho, Chiyoda-ku, Tokyo 102-0075, Japan

E-mail: tando@kenroku.kanazawa-u.ac.jp

Received 29 March 2008, in final form 29 April 2008
Published 12 August 2008
Online at stacks.iop.org/Nano/19/384009

Abstract
The diffusion of individual point defects in a two-dimensional streptavidin crystal formed on biotin-containing supported lipid bilayers was observed by high-speed atomic force microscopy. The two-dimensional diffusion of monovacancy defects exhibited anisotropy correlated with the two crystallographic axes in the orthorhombic *C*222 crystal; in the 2D plane, one axis (the *a*-axis) is comprised of contiguous biotin-bound subunit pairs whereas the other axis (the *b*-axis) is comprised of contiguous biotin-unbound subunit pairs. The diffusivity along the *b*-axis is approximately 2.4 times larger than that along the *a*-axis. This anisotropy is ascribed to the difference in the association free energy between the biotin-bound subunit–subunit interaction and the biotin-unbound subunit–subunit interaction. The preferred intermolecular contact occurs between the biotin-unbound subunits. The difference in the intermolecular binding energy between the two types of subunit pair is estimated to be approximately 0.52 kcal mol^{-1}. Another observed dynamic behavior of point defects was fusion of two point defects into a larger defect, which occurred much more frequently than the fission of a point defect into smaller defects. The diffusivity of point defects increased with increasing defect size. The fusion and the higher diffusivity of larger defects are suggested to be involved in the mechanism for the formation of defect-free crystals.

1. Introduction

Crystals, which are ordered lattices of colloids, molecules or atoms, have attracted much attention because of their wide range of applications in material science, biology and engineering. Although the constituents are assumed to be perfectly ordered in an ideal crystal, real crystals have numerous imperfections such as point defects, incorporated impurities, dislocations and grain boundaries. These crystal imperfections significantly affect, for example, the properties of semiconductors [1, 2] and limit the resolution of protein structures obtained by diffraction methods [3, 4]. Therefore, the behavior of lattice defects both in two-dimensional (2D) and three-dimensional (3D) crystals has been a subject of great interest in many fields.

Streptavidin is a homotetrameric protein with dihedral *D*2 symmetry, and each subunit specifically binds to one biotin [5, 6]. Streptavidin is easily crystallized in 2D forms on biotinylated lipid layers, which is considered to be an ideal model system for investigating 2D crystals grown on lipid layers [7, 8] and protein crystallization in general. On the biotinylated lipid layers, two of the four biotin binding

[1] Address for correspondence: Department of Physics, Kanazawa University, Kakuma-machi, Kanazawa 920-1192, Japan.

sites face the lipid layers and are occupied by biotin, while the other two are exposed to the aqueous environment and therefore are biotin-free. Thus far, it has been reported that ordered 2D arrays of streptavidin molecules are formed on biotinylated lipid layers at both the air–water [7–14] and solid–water [15–17] interfaces, the molecular arrangements of which have been investigated by transmission electron microscopy (TEM) [8–13] and atomic force microscopy (AFM) [14–16]. These studies have revealed that streptavidin molecules self-assemble in three distinct crystalline arrangements ($P1$, $P2$ and $C222$ symmetries), depending on the crystallization conditions such as pH [11, 13], ionic strength [12], and biotin concentration in the lipid membrane [16]. Here, the crystallographic symmetries are named following the nomenclature used in the literature [9, 13, 15]. It should be noted that $C222$ is the symmetry of the 2D crystal itself. In projection, the in-plane 2-fold rotational axes become mirror axes, and the symmetry of the projection map is *cmm*. As already mentioned, the streptavidin molecule itself possesses $D2$ (222 in the international system) point group symmetry [5, 6].

Streptavidin 2D crystals exhibit macroscopic morphologies resulting from the growth anisotropy. The dependence of the growth rate on the crystallographic axes has been attributed to a structural difference between biotin-bound and biotin-unbound subunits, which would result in heterogeneous intermolecular contacts in the crystals [9]. The relationship between the preferred crystal growth direction and the orientation of streptavidin molecules has been investigated by the combination of optical microscopy and electron microscopy. This relationship was first studied by Ku *et al* [9]. They proposed that the growth of the $C222$ crystal preferably occurs along the crystallographic axis along which biotin-free subunits are contiguously aligned. Therefore, the preferred intermolecular contact was assigned to be that between biotin-unbound subunits. Later, this model was revised by Wang *et al* [11]. They concluded that the faster growth of the $C222$ crystal occurs along the crystallographic axis in which biotin-bound subunits are contiguously aligned. Hence, the preferred intermolecular contact was assigned to that between biotin-bound subunits. Although this conclusion has been adopted in the literature, this issue still remains controversial.

The anisotropy of intermolecular interactions is expected to affect the dynamic behavior of individual constituent molecules and lattice defects in the crystal. The analysis of the dynamic behavior of individual point defects would offer insights into protein–protein interactions in crystals and crystal growth mechanisms. AFM is one of the most appropriate tools for the analysis of such dynamic behavior in protein crystals because of its applicability in liquid environments. Thus far, several attempts have been carried out to directly visualize the morphological changes in protein crystals by successive AFM imaging. For example, the crystal growth kinetics of a virus [4], lysozyme [18] and apoferritin [19] have been measured at a resolution close to the size of the molecules. However, because of its slow imaging speed, conventional AFM lacks the ability to track dynamic phenomena taking place on the 2D crystals at the single molecule level. For example, the attachment and detachment of apoferritin molecules at the growth steps on the crystal occur in a few seconds or less [19], while conventional tapping mode AFM requires at least a minute to obtain one image.

Here, we report defect diffusion in the orthorhombic $C222$ crystal of streptavidin formed on biotin-containing supported lipid bilayers. The 2D migration of defects was successfully traced by our high-speed AFM [20–23] at an imaging rate of 0.5 s/frame. The defects showed anisotropic diffusion with respect to the two crystal axes. An analysis of this anisotropic diffusion of monovacancy defects revealed different intermolecular binding affinities between a pair of biotin-unbound subunits and between a pair of biotin-bound subunits. In contrast to the result of a previous study by Wang *et al* [11], the preferred intermolecular contact in the crystal was between biotin-unbound subunits, which is consistent with the result obtained by Ku *et al* [9]. This conclusion was further confirmed by the observation that the ordered crystalline arrangement was immediately disrupted by the addition of biotin to the bulk solution. The difference in the intermolecular binding energy between the two types of subunit pair was estimated to be approximately 0.52 kcal mol^{-1}. In the AFM observation of the $C222$ crystal, we also found another interesting dynamic process: fusion of two point defects into a point defect. Its analysis suggested that the fusion and the higher mobility of the resulting larger defect are involved in the mechanism for the formation of defect-free crystals. In addition, we resolved the molecular arrangements in the $C222/P2$ coexisting crystals, which clarified the mechanism by which the $C222/P2$ coexisting crystal preferably grows in the same direction [11].

2. Materials and methods

2.1. Materials

All lipids used in this study were purchased from Avanti Polar Lipids (Alabaster, AL, USA). Streptavidin was purchased from Wako Pure Chemical (Osaka, Japan). Biotin (vitamin H) was purchased from Sigma (St Louis, MO, USA). These materials were used without further purification.

2.2. Sample preparation

Streptavidin 2D crystals were formed on the supported lipid bilayer (SLB) by slight modification of the method described in [15]. The lipid composition used in this study was dioleoylphosphatidylcholine (DOPC), dioleoylphosphatidylserine (DOPS) and 1,2-dioleoyl-*sn*-glycero-3-phosphoethanolamine-*N*-(cap-biotinyl) (biotin-cap-DOPE) (7:2:1, weight ratio). Dried lipid films were obtained by mixing appropriate amounts of lipids dissolved in chloroform followed by evaporating the solvent with argon. The lipid films were further dried in a desiccator by aspirating for more than 30 min. To obtain multilamellar vesicles (MLVs), the dried lipid films were resuspended by vortexing in a solution (buffer-A) containing 10 mM HEPES-NaOH, 150 mM NaCl, and 2 mM $CaCl_2$ (pH 7.4). Small unilamellar vesicles (SUVs) were produced from the MLV suspension by sonication with a tip-sonicator.

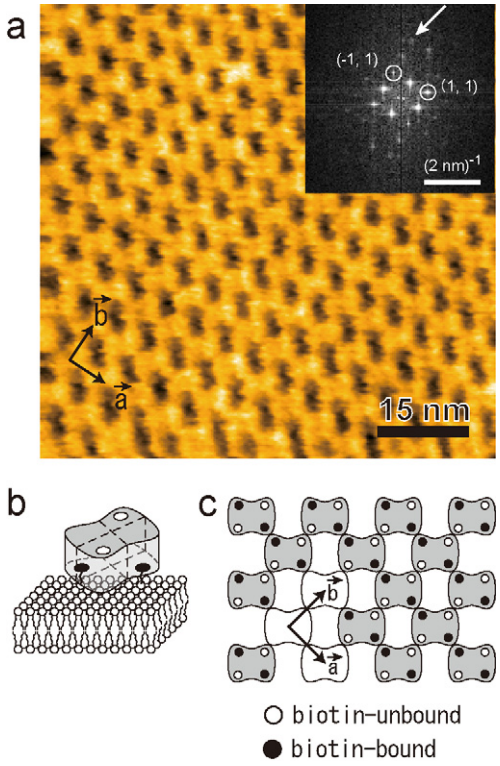

Figure 1. Streptavidin 2D crystal formed on a mica-supported lipid bilayer. (a) High-speed AFM image of a streptavidin crystal with $C222$ symmetry. In the inset, a calculated diffraction pattern of the AFM image is shown. The peak positions at (1, 1) and (−1, 1) are indicated by circles. The weakest measurable diffraction spot at (−1, 3) (1.9 nm resolution) is indicated by an arrow. (b) Schematic of a streptavidin molecule on a biotinylated lipid bilayer. Two biotin binding sites occupied by biotin are indicated by the closed circles. The open circles indicate biotin binding sites facing the aqueous solution and are biotin-free. (c) Schematic of streptavidin arrays in a $C222$ crystal. Unit lattice vectors are indicated: the a-axis includes rows of contiguous biotin-bound subunits, while the b-axis includes rows of contiguous biotin-unbound subunits.

SLBs were prepared by depositing 0.1 mg ml^{-1} SUVs onto a freshly cleaved mica surface, followed by incubation for 30 min in a chamber with saturated humidity at room temperature. Then, the excess lipids were washed out with a large amount of buffer-A.

The 2D crystallization of streptavidin was performed by placing a streptavidin solution (0.1 mg ml^{-1}) on the biotin-containing SLBs, followed by incubation for 2 h in a chamber with saturated humidity at room temperature. The buffer solutions used for the streptavidin crystallization were buffer-A for the $C222$ crystal and buffer-B (10 mM HEPES-NaOH, 300 mM NaCl and 2 mM $CaCl_2$ (pH 7.4)) for the $C222/P2$ coexisting crystal. The excess streptavidin molecules were washed out with the same buffer solution as that used for crystallization. By AFM observation, we confirmed that the streptavidin 2D crystals were uniformly formed over a ∼1 μm^2 area. Although a small amount of particles was found on the crystals, completely flat regions of ∼200 × 200 nm^2 area were observed elsewhere on the crystal samples. Therefore, this incompleteness of the crystal had no effect on our measurements.

To evaluate the effect of biotin binding on the intermolecular association in the crystal, biotin molecules were bound to all the available subunits of streptavidin. For this purpose, a buffer-A solution containing 1 mM biotin was injected to the AFM sample chamber while successively imaging the streptavidin 2D crystal sample, which resulted in the immediate disruption of the crystalline arrays (see section 3.3). Then, the excess biotin molecules were washed out with buffer-A. To test whether the crystal disordering upon full biotin binding is due to the lowered intermolecular binding affinity or partial dissociation of streptavidin from the lipid layer surface, the sample was further incubated for 1 h in a buffer-A solution containing 0.1 mg ml^{-1} of biotin-free streptavidin. For the chemical fixation of the crystals, a buffer-A solution containing 10 mM glutaraldehyde was added, followed by incubation for 5 min.

2.3. High-speed atomic force microscopy

The observations of streptavidin 2D crystals were performed in tapping mode using a laboratory-built high-speed atomic force microscope [20, 24, 25]. Small cantilevers designed for high-speed AFM were used, which have a spring constant of 0.1–0.2 N m^{-1}, a resonant frequency of 0.8–1.2 MHz in water, and a quality factor of ∼2 in water [26]. The cantilever tips were grown by electron beam deposition. The condition for imaging defect diffusion was typically as follows. The cantilever's free oscillation peak-to-peak amplitude was set to 5 nm, while the set-point peak-to-peak amplitude during imaging was 4–4.5 nm. The scan area was 150 × 150 nm^2, and the number of pixels was 200 × 200. The imaging rate was 0.5 s/frame. The amplitude error signal was negligibly small during scanning, indicating that the feedback speed is sufficiently high to precisely trace the surface topography. The substrate-tilt effect was removed from the AFM images by a flattening software program. The scan size in the x- and y-directions was calibrated using purple membranes as a standard specimen, which are 2D crystals of bacteriorhodopsin with a spacing of 6.2 nm between unit cells [27].

3. Results

3.1. Streptavidin 2D crystal with C222 symmetry

Figure 1(a) shows AFM images of a streptavidin 2D crystal. The periodic structure exhibits $C222$ symmetry with lattice constants of $a = 5.9 \pm 0.1$ nm, $b = 5.9 \pm 0.3$ nm, and $\gamma = 92 \pm 3°$. These values are consistent with the previously reported result of $a = 5.8$ nm, $b = 5.8$ nm, and $\gamma = 90°$ for a $C222$ crystal prepared at the air/water interface [13]. The calculated diffraction pattern indicated lateral resolution better than 2 nm (figure 1(a), inset). With this lateral resolution, the orientation of the rectangular streptavidin molecules was clearly identified. Owing to the dihedral $D2$ symmetry of tetrameric streptavidin, the two biotin binding sites facing the lipid membrane are occupied by biotin, while the other two are unoccupied (figure 1(b)). Thus, the arrangement of biotin-bound and biotin-unbound subunits in the crystal axis coordinates can be determined in the AFM images. Figure 1(c)

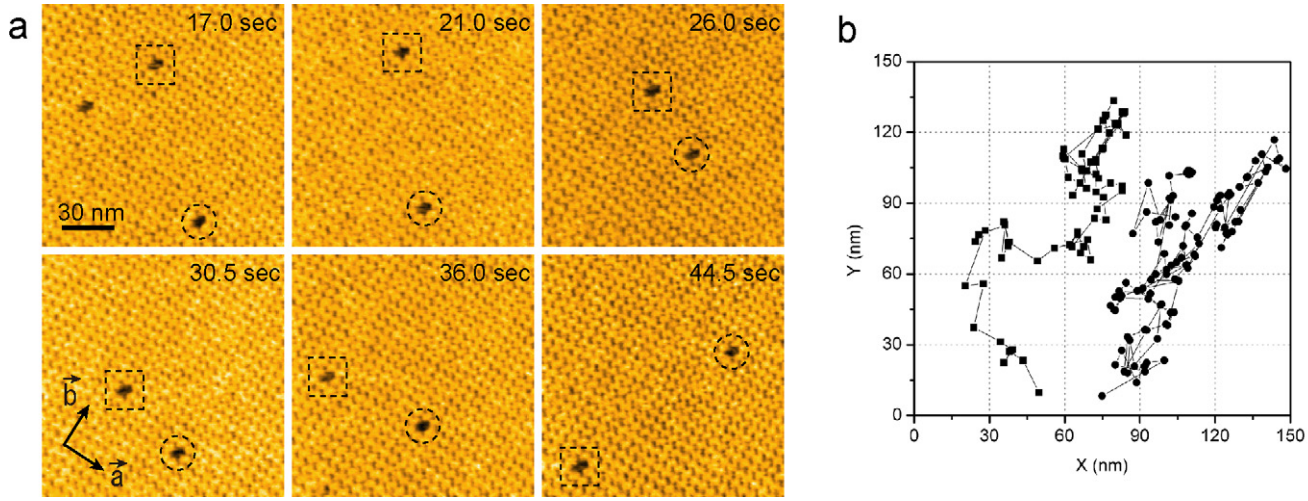

Figure 2. Migration of monovacancy defects in streptavidin 2D crystal. (a) High-speed AFM images of streptavidin 2D crystal and monovacancy defects therein. The monovacancy defects are enclosed by dashed squares and circles. The directions of the lattice vectors of the crystal are also indicated. Successive images were obtained at an imaging rate of 0.5 s/frame with a scan area of 150 × 150 nm^2, and the number of pixels was 200 × 200. (b) Trajectories of individual monovacancy defects. Closed squares and circles correspond to defects indicated by open squares and circles shown in (a), respectively.

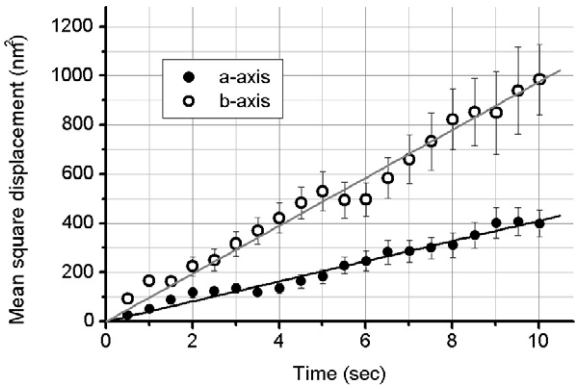

Figure 3. Plot of mean-square displacements (MSDs) of monovacancy defects against time. The MSDs as a function of time were measured from 94 trajectories. Error bars indicate standard error. The MSDs of defects along the *a*-axis and the *b*-axis in the *C*222 crystal are compared. Data fitted to a linear function yielded diffusion constants $D_a = 20.5$ nm^2 s^{-1} and $D_b = 48.8$ nm^2 s^{-1} for the directions along the *a*-axis and the *b*-axis, respectively. Closed circle, MSDs with the *a*-axis that includes rows of contiguous biotin-bound subunits; open circle, MSDs with the *b*-axis that includes rows of contiguous biotin-unbound subunits.

shows a schematic of the molecular arrangement in the *C*222 crystal. In the *C*222 crystal, the intermolecular contacts between biotin-bound subunits are contiguously aligned along one crystal axis (the *a*-axis), while the contacts between biotin-unbound subunits are contiguously aligned along the other axis (the *b*-axis).

3.2. Diffusion of point defects in crystal

Monovacancy defects in the streptavidin 2D crystals were produced by increasing the tapping force onto the sample from the oscillating tip, similarly to a method used previously [28]. Then, the diffusion of point defects in the crystals was observed. Figure 2(a) shows images of the streptavidin 2D crystal and monovacancy defects therein, which are clipped from successively captured high-speed AFM images. In figure 2(b), the trajectories of two monovacancy defects are shown. The mobility of the monovacancy defects was obviously anisotropic with respect to the two axes of the crystalline lattice. These defects have larger mobility along the *b*-axis than along the *a*-axis. Occasionally, the defects stopped diffusing at lattice sites. While observing the crystal for several seconds, the stopped defects started to diffuse again. This behavior may arise from the discontinuity of the SLB underneath the streptavidin crystal. The total time in which the defects are arrested at lattice sites was ∼3% of the total observation time, which is negligibly small to affect our analyses of the defect diffusion.

The mobility of monovacancy defects along each axis of the *C*222 crystal was quantified by measuring the mean-square displacements (MSDs) at various intervals (figure 3). From the linear increase in MSDs with time, the diffusion rate constants of migrating monovacancy defects were $D_a = 20.5$ nm^2 s^{-1} along the *a*-axis that includes rows of contiguous biotin-bound subunits, and $D_b = 48.8$ nm^2 s^{-1} along the *b*-axis that includes rows of contiguous biotin-unbound subunits. D_a and D_b are similar even for other samples that have different orientations of the crystal axes relative to the raster scan direction. Thus, we conclude that the anisotropy in diffusivity is an intrinsic property of the lattice defects in the streptavidin *C*222 crystal.

The monovacancy defects sometimes fused into a bivacancy defect. Through several fusions, larger multivacancy defects were formed. The multivacancy defects also diffused in the *C*222 crystals during the successive imaging. In figure 4, the diffusion constants of the multivacancy defects are shown as a function of the defect size. As the size increases, the diffusivity of multivacancy defects increases for both crystal axes, although the diffusivity of divacancy defects is similar

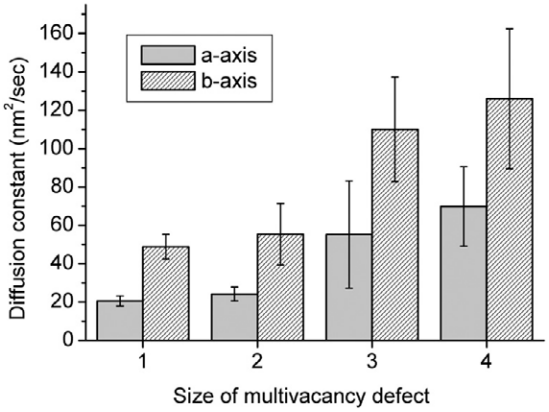

Figure 4. Diffusion constants of multivacancy defects for each axis as a function of the defect size. Each number (as an index of the defect size) indicates the number of unit vacant sites contained in each multivacancy defect. Error bars indicate standard error.

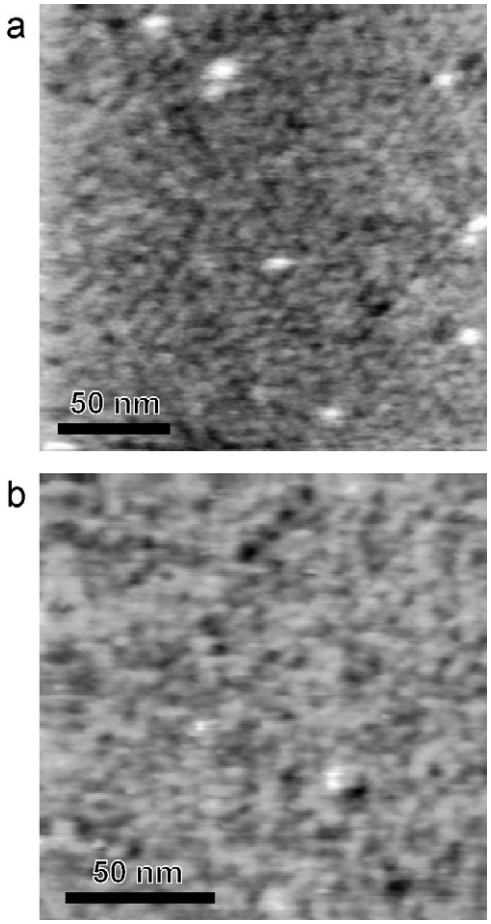

Figure 5. Disruption of crystalline lattice of streptavidin on full binding to biotin. (a) Molecular arrangements of streptavidin after biotin binding at all available binding sites. (b) Molecular arrangements of streptavidin after incubating the sample shown in (a) in the presence of biotin-free streptavidin.

to that of monovacancy defects. Interestingly, the reverse reaction, i.e., fission of a large multivacancy defect to smaller multivacancy or monovacancy defects, was rarely observed.

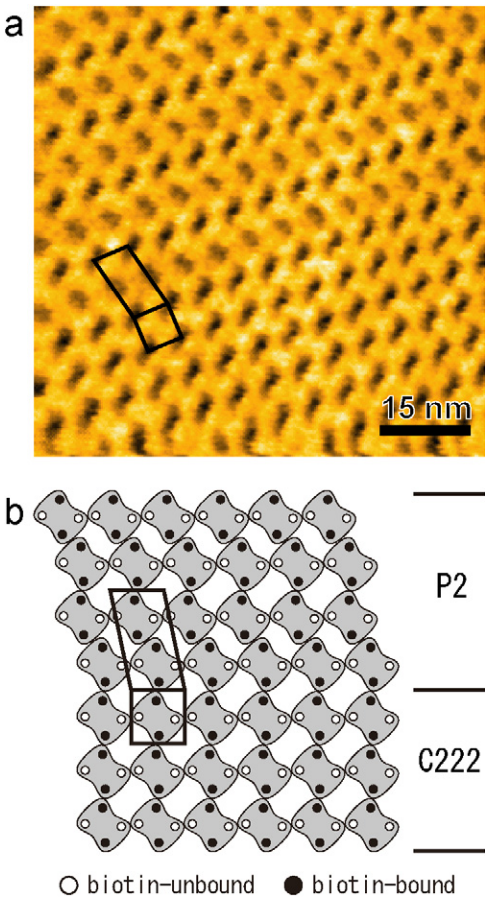

Figure 6. Molecular arrangements at the boundary of $C222$ and $P2$ domains. (a) High-speed AFM image of a streptavidin $C222/P2$ coexisting crystal, which was grown in a high ionic solution (buffer-B). The lower region of the image shows $C222$ arrangement, while the $P2$ lattice is seen at the upper region. (b) Schematic of streptavidin arrays in the $C222/P2$ coexisting crystal. Unit cells in the $C222$ and $P2$ regions are indicated by a square and parallelogram, respectively. The $C222$ and $P2$ crystals are connected through the interaction between biotin-bound subunits at their interface.

3.3. Influence of biotin binding to ordered arrays of streptavidin

When the crystals were exposed to free biotin in the bulk solution, the ordered lattices were immediately disrupted. After the disruption, the individual streptavidin molecules were undetectable without chemical fixation because of the rapid diffusion of the streptavidin molecules on the SLBs. After the fixation with glutaraldehyde, the surface structures could be observed owing to the elimination of the lateral movement of streptavidin molecules. From figure 5(a), it is clear that streptavidin molecules are densely packed on the mica-supported lipid membranes but are arranged in a disordered structure. The disordered structure, which was not treated with glutaraldehyde, failed to recover to an ordered lattice after incubation in a biotin-free solution containing streptavidin (figure 5(b)), indicating that the streptavidin had never dissociated from the biotinylated lipids by the addition of biotin to the bulk solution.

3.4. Molecular arrangements in C222/P2 coexisting crystal

By increasing the ionic strength of the crystallization buffer, $C222/P2$ coexisting crystals were obtained. Figure 6(a) shows an AFM image of the boundary between the $C222$ and $P2$ regions in a coexisting crystal. The lattice constants of the $P2$ crystal domain were $a = 5.8 \pm 0.1$ nm, $b = 11.2 \pm 0.3$ nm, and $\gamma = 104° \pm 1°$, which agree with those reported in a previous work [10]. Figure 6(b) shows a schematic of the molecular arrangements in the $C222/P2$ coexisting region modeled from figure 6(a). Streptavidin molecules in the $C222$ domain appear oriented in the same direction as that in the adjacent $P2$ crystal. This result is consistent with the fact that the $C222$ and $P2$ regions grow in the same preferred direction [11].

4. Discussion

4.1. Observations of point defect diffusion in a crystal by high-speed AFM

The migration of monovacancy defects in the streptavidin 2D crystals was visualized by high-speed AFM, as shown in figure 2. The linear relationship between MSDs and time (figure 3) of this migration indicates that the migration of monovacancy defects occurs by a random walk. The one-dimensional diffusion constant D is expressed as $D = \delta^2/2\tau$, where δ is the step length and τ is the time for each step (stepping time) [29]. In the $C222$ crystal of streptavidin, the step length δ is 5.9 nm in both two axes because the minimum step length corresponds to the lattice constant. Therefore, the stepping time τ for the movements along each axis can be estimated to be $\tau_a = 0.85$ s and $\tau_b = 0.36$ s for the a-axis and the b-axis, respectively. In this study, the imaging rate was 0.5 s/frame, which is comparable to the stepping rates of monovacancy defects in the crystal. Thus, the trajectories of individual monovacancy defects diffusing in the 2D crystal were well traced.

4.2. Anisotropic diffusion along two axes

In the $C222$ crystal of streptavidin, the two-dimensional diffusion of monovacancy defects showed significant anisotropy correlated with the two crystal axes, as indicated in figures 2 and 3. This anisotropy in the lateral mobility (i.e., $D_b > D_a$) arises from a free energy difference between the biotin-bound subunit–subunit interaction and biotin-unbound subunit–subunit interaction. When a streptavidin molecule adjacent to a monovacancy defect moves to the defect site along the a-axis, two intermolecular bonds between biotin-unbound subunits ('u–u bond') and one intermolecular bond between biotin-bound subunits ('b–b bond') are broken. On the other hand, when it moves to the defect site along the b-axis, one u–u bond and two b–b bonds are broken (see figure 1(c)). Therefore, the difference in the activation energies E_a and E_b for the step movement of a monovacancy defect along the respective a- and b-axes simply corresponds to the difference between the free energy changes $G_{\mathrm{u–u}}$ and $G_{\mathrm{b–b}}$ produced by the formation of the respective u–u bond and b–b bond; namely, $E_b - E_a = G_{\mathrm{u–u}} - G_{\mathrm{b–b}}$. Therefore, the observed relationship $D_b > D_a$ indicates $G_{\mathrm{u–u}} < G_{\mathrm{b–b}}$; namely, the u–u bond affinity is higher than that of the b–b bond. The ratio of the two diffusion rate constants (D_b/D_a) can be expressed by $D_b/D_a = \exp[-(E_b - E_a)/(k_{\mathrm{B}}T)]$, where k_{B} is the Boltzmann constant and T is the absolute temperature. Thus, from the observed value of $D_b/D_a \sim 2.4$, the free energy difference $G_{\mathrm{u–u}} - G_{\mathrm{b–b}}$ is estimated to be approximately $-0.88 k_{\mathrm{B}}T$ ($T \sim 300$ K), which corresponds to -0.52 kcal mol^{-1}.

In previous studies, the anisotropy of protein 2D crystal growth has been evaluated from the crystal morphologies. The streptavidin $C222$ crystals formed under biotinylated lipid layers show X-, H-, and rectangle-shaped morphologies [8, 9, 11, 13] that arise from asymmetric growth rates along perpendicular axes. The anisotropy estimated from the aspect ratios of the $C222$ crystals is reported to be 2–3 (about 2 at neutral pH) [13], coinciding with the diffusion constant ratio ($D_b/D_a \sim 2.4$). We think that this coincidence is accidental. However, it is obvious that the diffusion constant ratio is intrinsically related to the anisotropic growth rate through the free energies associated with the attractive intermolecular interactions between the subunits [30]. Supposing that the aspect ratio of a crystal is proportional to the ratio of the free energies of attractive interactions that occur along the crystal axes (Wulff's rule [31]), $G_{\mathrm{u–u}}/G_{\mathrm{b–b}}$ is approximately 2. This relationship and $G_{\mathrm{u–u}} - G_{\mathrm{b–b}} \sim -0.88\, k_{\mathrm{B}}T$ result in $G_{\mathrm{b–b}} \sim -0.88\, k_{\mathrm{B}}T$ and $G_{\mathrm{u–u}} \sim -1.76\, k_{\mathrm{B}}T$. These values seem consistent with the fact that 2D protein crystallization requires lateral interaction energies between -1 and $-5\, k_{\mathrm{B}}T$. Although this estimation of the interaction energies cannot be validated at present, it will be cleared by systematic studies on the monovacancy defect mobility in the other types of streptavidin 2D crystals formed under various conditions.

4.3. Fusion of point defects

Fusion of two point defects into a larger point defect was often observed. On the other hand, fission of a multivacancy point defect into smaller point defects was rarely observed. We think that the fission often occurs but cannot easily be observed because the two point defects formed immediately after the fission are quickly fused again. Immediately after the fission, a streptavidin molecule becomes facing both the resulting two smaller point defects. This streptavidin molecule contains only two intermolecular subunit–subunit contacts, and therefore quickly detaches from the lattice and moves into either of the two adjacent point defects. The imaging rate we used (0.5 s/frame) was not sufficiently high to observe this transiently occurring fission.

During the formation of streptavidin 2D crystals in the presence of free streptavidin in the bulk solution, small point defects such as monovacancy and divacancy defects would not easily have access to the free streptavidin molecules, and hence, they have a tendency to remain in the crystals. However, the fusion of small point defects into a larger point defect facilitates its access to the free streptavidin molecules and thereby promotes the removal of small point defects from the crystals.

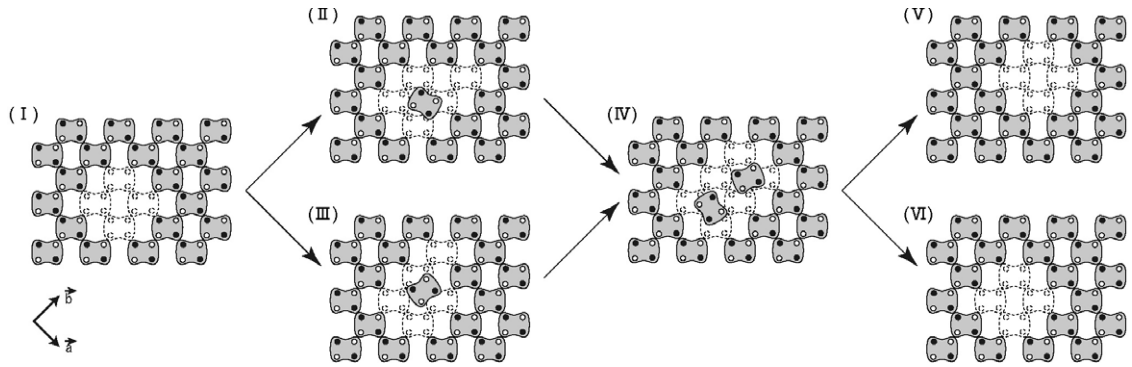

Figure 7. Pathways for the step movement of a cross-shaped tetravacancy point defect to the $+b$ direction. The defects are schematically indicated with broken lines. (I): the initial state of a cross-shaped tetravacancy point defect; (II) and (III): the initial transient states; (IV): the second transient state; (V) and (VI): the final states. In state (V), the step movement in the $+b$ direction is attained, while state (VI) is the same as the initial state (I).

4.4. Increased diffusivity of multivacancy defects in a crystal

As shown in figure 4, the defect mobility increases with increasing defect size. It does not seem easy to interpret this tendency intuitively as more than three intermolecular bonds between streptavidin molecules are involved in the diffusion of the multivacancy defects. The total number of intermolecular bonds to be broken for the defect step movement increases with increasing size of vacancy. This fact seems contrary to the observed tendency (faster diffusion with larger defect).

This conflict could be resolved by considering two factors. One factor is that there are multiple paths along which a multivacancy defect migrates to one of their nearest-neighbor positions. For simplicity, let us consider the step movement of a cross-shaped tetravacancy defect in the $+b$ direction (figure 7). In the initial step, one of the two streptavidin molecules, which face the defect and locate in the $+b$ direction relative to the defect, detaches from the surrounding crystal region (steps from (I) to (II) and from (I) to (III) in figure 7). In this detachment, three intermolecular bonds are broken. Once detached, one of streptavidin molecules, which had been in contact with the detached streptavidin molecule, loses one b–b bond, resulting in two intermolecular bonds. Therefore, it quickly detaches from the surrounding crystal region (steps from (II) or (III) to (IV) in figure 7). The two detached streptavidin molecules rapidly diffuse in the void and quickly reach the stable configurations ((V) or (VI) in figure 7). In these pathways, the initial steps, from (I) to (II) or from (I) to (III), limit the rate of the defect step movement. Compared with the step movement of a monovacancy defect, the step movement of a cross-shaped tetravacancy defect has two parallel paths for the initial rate-limiting step. Therefore, its diffusivity is approximately twice as fast as that of a monovacancy defect.

Another factor to be considered for the movement of a multivacancy point defect is the stability of the crystal regions surrounding the point defect. By a collective effect, the stability of the crystal regions adjacent to a larger point defect must be lower than that of crystal regions adjacent to a smaller defect. This lower stability gives higher diffusivity to larger point defects.

The higher mobility of larger point defects increases their probability to encounter other point defects to form larger point defects with further higher mobilities. During the crystal growth in the presence of free streptavidin in the bulk solution, this acceleration effect also promotes the removal of point defects from the crystalline regions.

4.5. Discrepancy in preferred intermolecular interaction with previous study

In the study by Wang *et al* [11], the preferred crystal growth direction was examined by the observation of the macroscopic crystal morphology by fluorescent microscopy, while the molecular arrangement in the crystal was analyzed by TEM and electron diffraction. In this manner, the preferred intermolecular contact was determined. In our study, the molecular arrangement and the diffusion of point defects in the crystal were simultaneously visualized by high-speed AFM, and the preferred intermolecular contact was determined by analyzing the anisotropic diffusion of monovacancy defects in the lattice structure. As proposed by Ku *et al* [9], the results of our study indicate that the preferred intermolecular contact in the $C222$ crystal is between biotin-unbound subunits, contradicting with the report by Wang *et al*. Unfortunately, it is likely that Wang *et al* have incorrectly assigned the streptavidin orientation in the $C222$ crystal. As shown in figure 1(a) (inset), the calculated diffraction pattern of the $C222$ crystal exhibits a higher intensity at the (1, 1) peak than at the $(-1, 1)$ peak. The vectors (1, 1) and $(-1, 1)$ correspond to the directions of the long and short axes of the rectangle-shaped streptavidin, respectively. This result was confirmed by the calculated diffraction pattern of a $C222$ lattice of an artificial rectangle molecule constituted in a computer. In contrast to our observation, in the report of Wang *et al*, the electron diffraction intensities and the determined molecular orientation are inconsistent with each other.

Further support for our conclusion as to the preferred intermolecular contact is first provided from our observation that the $C222$ crystal is immediately disordered upon the addition of biotin to the sample solution. Second, it is provided from the observation of the $C222/P2$ coexisting

crystal. The high-speed AFM imaging of the $C222/P2$ coexisting crystal showed that streptavidin molecules in the $C222$ and $P2$ domains are oriented in the same direction (figure 6). From this result, we can anticipate that the $C222$ and $P2$ domains preferentially grow in the same direction by sharing the same orientation of the preferred intermolecular contact between biotin-unbound subunits. In fact, it has been observed that the $C222/P2$ coexisting crystal grows in the same direction [11]. In a model provided by Wang *et al*, this fact was interpreted based on (1) in the coexisting crystal, the orientations of streptavidin molecules in the $C222$ and $P2$ regions are different by 90°, and (2) the preferred intermolecular contact in the $C222$ region is between biotin-bound subunits while that in the $P2$ region is between biotin-unbound subunits. It is very unlikely that, under the same solution condition, the preferred intermolecular contacts are different at the two crystal regions.

4.6. Implication for intermolecular contact in a C222 crystal

Among various 2D crystals of streptavidin and its mutants formed on lipid layers, symmetric square-shaped crystals with $C222$ symmetry have been obtained. For example, they are formed on biotin-containing lipid layers using streptavidin mutants (T20A [32] and N23A [33]). In these crystals, the affinity of the intermolecular contacts between subunits is considered independent of the biotin binding. Since the amino acid residues T20, W21 and Y22 are involved in hydrogen-bond interaction at the intermolecular contact interface in the $C222$ crystal, the mutation (from T20 to A20) is considered to suppress the structural changes in the interface induced by biotin binding. N23 is a key element for hydrogen-bonding to biotin, and therefore, the mutation (from N23 to A23) significantly lowers the affinity for biotin [33]. In addition, N23 is adjacent to the intermolecular contact interface in the $C222$ crystal. This significantly low affinity for biotin is likely to decouple the biotin binding and the structural changes in the intermolecular contact interface; namely, the binding of biotinylated lipid to N23A streptavidin does not weaken the intermolecular subunit contact in the $C222$ crystal. This decoupling results in the symmetric crystal growth in the two orthogonal directions. In fact, the square-shaped $C222$ crystal of N23A streptavidin exhibits a significantly low critical surface concentration for crystallization, whereas different mutants with relatively high affinities for biotin produce asymmetric $C222$ crystals with higher critical surface concentration [33].

5. Conclusion

In this study, we introduced a completely new approach to the analysis of protein 2D crystallization under lipid layers. We measured the diffusion of point defects in the visualized streptavidin 2D crystal lattice, using high-speed AFM. The molecular arrangement in the crystal was directly obtained owing to the spatial resolution better than 2 nm. The point defects exhibited anisotropic diffusion with respect to the two crystal axes. This anisotropy is related to the asymmetric crystal growth along the crystal axes. Quantitative evaluation of this relationship and finding its general rule remain important issues to elucidate. From the visualized anisotropic diffusion of monovacancy defects and the molecular arrangement, the difference in the free energy between the biotin-bound subunit–subunit interaction and the biotin-unbound subunit–subunit interaction was determined to be 0.52 kcal mol^{-1}; the contact between biotin-bound subunits is weaker than that between biotin-unbound subunits. In addition, the rapid disruption of the ordered lattice upon the addition of free biotin was observed. The fusion of point defects occurs much more predominantly over the fission of a point defect into smaller point defects. The higher mobility of larger point defects increases the probability of the fusion event and thereby accelerates the removal of point defects during crystallization in the presence of free streptavidin in the bulk solution. The molecular arrangements in the $C222/P2$ coexisting crystals were revealed, which cleared the mechanism by which the $C222/P2$ coexisting crystal grows in the same preferred direction. These results show that high-speed AFM developed by us for the studies of dynamic behavior of biomolecular machines at work [21] is also useful for studying various dynamic processes in protein 2D crystallization, such as the nuclear formation, the initial growth process, the fusion of small crystal patches, the defect exclusion process and the growth process of a different-symmetries-coexisting crystal.

Acknowledgments

We thank Hayato Yamashita for providing us with a purified purple membrane sample. This work was supported by the CREST project (to TA), the project of Development of System and Technology for Advanced Measurement and Analysis (to TA), and Strategic International Cooperative Program (to TU) of the Japanese Science and Technology Agency, and a Grant-in-Aid for Basic Research (S) from the Ministry of Education, Culture, Sports, Science, and Technology of Japan (to TA).

References

[1] Queisser H J and Haller E E 1998 Defects in semiconductors: some fatal, some vital *Science* **281** 945–50
[2] Coey J M D, Venkatesan M and Fitzgerald C B 2005 Donor impurity band exchange in dilute ferromagnetic oxides *Nat. Mater.* **4** 173–9
[3] Chernov A A 2003 Protein crystals and their growth *J. Struct. Biol.* **142** 3–21
[4] Malkin A J and McPherson A 2002 Novel mechanisms for defect formation and surface molecular processes in virus crystallization *J. Phys. Chem.* B **106** 6718–22
[5] Weber P C, Ohlendorf D H, Wendoloski J J and Salemme F R 1989 Structural origins of high-affinity biotin binding to streptavidin *Science* **243** 85–8
[6] Hendrickson W A, Pähler A, Smith J L, Satow Y, Merritt E A and Phizackerley R P 1989 Crystal structure of core streptavidin determined from multiwavelength anomalous diffraction of synchrotron radiation *Proc. Natl Acad. Sci. USA* **86** 2190–4
[7] Blankenburg R, Meller P, Ringsdorf H and Salesse C 1989 Interaction between biotin lipids and streptavidin in

monolayers: formation of oriented two-dimensional protein domains induced by surface recognition *Biochemistry* **28** 8214–21
[8] Darst S A, Ahlers M, Meller P H, Kubalek E W, Blankenburg R, Ribi H O, Ringsdorf H and Kornberg R D 1991 Two-dimensional crystals of streptavidin on biotinylated lipid layers and their interactions with biotinylated macromolecules *Biophys. J.* **59** 387–96
[9] Ku A C, Darst S A, Robertson C R, Gast A P and Kornberg R D 1993 Molecular analysis of two-dimensional protein crystallization *J. Phys. Chem.* **97** 3013–6
[10] Wang S-W, Poglitsch C L, Yatcilla M T, Robertson C R and Gast A P 1997 Solid phase coexistence in chiral domains of two-dimensional streptavidin crystals *Langmuir* **13** 5794–8
[11] Wang S-W, Robertson C R and Gast A P 1999 Molecular arrangement in two-dimensional streptavidin crystals *Langmuir* **15** 1541–8
[12] Ratanabanangkoon P and Gast A P 2003 Effect of ionic strength on two-dimensional streptavidin crystallization *Langmuir* **19** 1794–801
[13] Yatcilla M T, Robertson C R and Gast A P 1998 Influence of pH on two-dimensional streptavidin crystals *Langmuir* **14** 497–503
[14] Scheuring S, Müller D J, Ringler P, Heymann J B and Engel A 1999 Imaging streptavidin 2D crystals on biotinylated lipid monolayers at high resolution with the atomic force microscope *J. Microsc.* **193** 28–35
[15] Reviakine I and Brisson A 2001 Streptavidin 2D crystals on supported phospholipid bilayers: toward constructing anchored phospholipid bilayers *Langmuir* **17** 8293–9
[16] Lou C, Wang Z and Wang S-W 2007 Two-dimensional protein crystals on a solid substrate: effect of surface ligand concentration *Langmuir* **23** 9752–9
[17] Calvert T L and Leckband D 1997 Two-dimensional protein crystallization at solid–liquid interfaces *Langmuir* **13** 6737–45
[18] Durbin S D and Carlson W E 1992 Lysozyme crystal growth studied by atomic force microscopy *J. Cryst. Growth* **122** 71–9
[19] Yau S-T, Petsev D N, Thomas B R and Vekilov P G 2000 Molecular-level thermodynamic and kinetic parameters for the self-assembly of apoferritin molecules into crystals *J. Mol. Biol.* **303** 667–78
[20] Ando T, Kodera N, Takai E, Maruyama D, Saito K and Toda A 2001 A high-speed atomic force microscope for studying biological macromolecules *Proc. Natl Acad. Sci. USA* **98** 12468–72
[21] Ando T, Uchihashi T, Kodera N, Miyagi A, Nakakita R, Yamashita H and Sakashita M 2006 High-speed atomic force microscopy for studying the dynamic behavior of protein molecules at work *Japan. J. Appl. Phys.* 1 **45** 1897–903
[22] Ando T, Uchihashi T, Kodera N, Yamamoto D, Taniguchi M, Miyagi A and Yamashita H 2007 High-speed atomic force microscopy for observing dynamic biomolecular processes *J. Mol. Recognit.* **20** 448–58
[23] Ando T, Uchihashi T, Kodera N, Yamamoto D, Miyagi A, Taniguchi M and Yamashita H 2008 High-speed AFM and nano-visualization of biomolecular processes *Pflügers Arch.* **456** 211–25
[24] Kodera N, Yamashita H and Ando T 2005 Active damping of the scanner for high-speed atomic force microscopy *Rev. Sci. Instrum.* **76** 053708
[25] Kodera N, Sakashita M and Ando T 2006 Dynamic proportional-integral-differential controller for high-speed atomic force microscopy *Rev. Sci. Instrum.* **77** 083704
[26] Kitazawa M, Shiotani K and Toda A 2003 Batch fabrication of sharpened silicon nitride tips *Japan. J. Appl. Phys.* 1 **42** 4844–7
[27] Henderson R, Baldwin J M, Ceska T A, Zemlin F, Beckmann E and Downing K H 1990 Model for the structure of bacteriorhodopsin based on high-resolution electron cryo-microscopy *J. Mol. Biol.* **213** 899–929
[28] Yau S-T, Thomas B R and Vekilov P G 2000 Molecular mechanisms of crystallization and defect formation *Phys. Rev. Lett.* **85** 353–6
[29] Berg H C 1993 *Random Walks in Biology* (Princeton, NJ: Princeton University Press)
[30] Zhdanov V P, Höök F and Kasemo B 2001 Simulation of two-dimensional streptavidin crystallization *Proteins Struct. Funct. Genet.* **43** 489–98
[31] Wulff G 1901 Zur Frage der Geschwindigkeit des Wachstums und der Auflösung der Kristallflächen *Z. Kristallogr. Mineral.* **34** 449–530
[32] Edwards T C, Malmstadt N, Koppenol S, Hara M, Vogel V and Stayton P S 2002 Molecular basis for asymmetrical growth in two-dimensional streptavidin crystals *Langmuir* **18** 7447–51
[33] Koppenol S, Klumb L A, Vogel V and Stayton P S 1999 Effects of interfacial binding kinetics on two-dimensional streptavidin crystallization *Langmuir* **15** 7125–9